J Mater Sci (2009) 44:1394–1403
DOI 10.1007/s10853-006-1415-7

Transformation characteristics of ductile iron austempered from intercritical austenitizing temperature ranges

Mehmet Erdogan · Volkan Kilicli · Bilge Demir

Received: 2 April 2005 / Accepted: 22 February 2006 / Published online: 5 January 2007

Abstract In the present work, the transformation characteristics of ductile iron austempered from intercritical austenitization temperature ranges were investigated. For this purpose, an unalloyed ductile cast iron containing 3.50 wt% C, 2.63 wt% Si and 0.318 wt% Mn were intercritically austenitized (partially austenitized) at various temperatures and then rapidly transformed to a salt bath held at the 365 °C for austempering for various times to produce dual matrix structure with different ausferrite volume fractions in ferrite matrix. A microstructure map was created to illustrate the transformation of products quantitatively as a function of austempering time for a particular intercritical and austempering heat treatment temperature and time. It was demonstrated that the total volume fraction of transformed phases was approximately constant for all austempering times after rapidly transforming samples from a particular intercritical temperature to austempering temperature. It was found out that the new ferrite (It is also called epitaxial ferrite) introduced into the intercritically austenitized structure during austempering and its content was dependent on the intercritical austenitizing temperature and austempering time.

M. Erdogan (✉) · V. Kilicli
Materials Division, Metallurgy Education Department, Faculty of Technical Education, Gazi University, 06500 Besevler-Ankara, Turkey
e-mail: mehmeter@gazi.edu.tr

B. Demir
Materials Division, Metallurgy Education Department, Faculty of Technical Education, Zonguldak Karaelmas University, Karabuk, Turkey

Introduction

In the newly developed ductile cast iron [1–9] with dual matrix structure, the structure consists of proeutectoid ferrite, and ausferrite (bainitic ferrite and high-carbon austenite (it is also called retained, stable or transformed austenite)) or martensite. Therefore it is also called dual matrix structure (DMS) [1–4].

Austempered ductile iron (ADI) with DMS has been found to be validated for suspension parts of the automotive, owing to its greater ductility than the conventionally heat treated ADI. This material exhibits tensile and proof stress, together with hardness, similar to pearlitic grades, and ductility at the same level as ferritic grades.

In those studies [1, 2, 4–8], DMS was obtained by rapidly heating ductile iron into the single-phase (γ) region and then holding the material at this temperature for a very short time (generally less then 1 min) and then rapidly transforming the material to the austempering temperature or quenching the material to room temperature before the growth of austenite into surrounding ferrite was completed. The shortcoming of this heat treatment procedure is the control the volume fraction of phases.

Recently Cerah et al. [3] produced DMS with different martensite volume fraction distributed in soft proeutectoid ferrite matrix by controlled quenching from the intercritical austenitizing temperature (ICAT) range. They showed that the austenite volume fraction and its carbon content during intercritical austenitizing can be controlled preciously.

To date no attempts have been made to control ausferrite and proeutectoid ferrite volume fractions in

ADI with DMS. In the present study, DMS structures were obtained by austempering the ductile cast iron from the ICAT ranges (two-phase region ($\alpha + \gamma$)) and ausferrite and proeutectoid volume fractions and austenite carbon content were controlled by varying ICAT and austempering time. The ICAT ranges indicated here correspond to the $\alpha + \gamma$ + graphite region. In this article, this is indicated as the ($\alpha + \gamma$) temperature range.

In the existing ADI literature the ferrite in ADI structure is generally classified into two groups namely proeutectoid ferrite and bainitic ferrite [10]. During austempering, proeutectoid ferrite formed at ICAT remained untransformed but bainitic ferrite transformed from austenite.

The ICAT and austempering time affected the new ferrite (It is also called epitaxial ferrite) and high-carbon austenite content of austempered ductile cast iron. It was proposed that microstructure maps may be interpreted to obtain austenite $\rightarrow$ new ferrite content or austenite $\rightarrow$ high-carbon austenite of ductile cast iron data specific to different austenite contents formed during intercritical austenitizing. The percentage of high-carbon austenite which transformed to the new ferrite or high-carbon austenite was plotted as a function of the austempering time.

Experimental procedure

The chemical composition of the cast unalloyed ductile cast iron used in the present study is given in Table 1. The ductile iron was produced in a medium frequency induction furnace in a commercial foundry. The tundish cover ladle method was used to treat a 250 kg melt of iron with 6–7% Mg containing ferrosilicon alloy at 1,450 °C. Final inoculation was carried out with a 75% ferrosilicon alloy. The melt at the temperature between 1,400 and 1,450 °C was cast into Y-block sand mould which was prepared in accordance with ISO 1083. As cast structure was labelled as ''A'' for further reference. The microstructures of the specimen A was the starting point for subsequent heat treatment.

The preliminary investigation was to determine the dependence of austenite (martensite at room temperature) volume fraction on ICAT. For this purpose samples 10 mm × 10 mm × 5 mm thick machined from bottom section of the Y-block were annealed for 20 min in normal atmosphere at a series of temperatures from 780 to 845 (C for the Ae_1 and upper critical temperature, respectively (Fig. 1) and then quenched into water held at room temperature. Ae_1 temperature limits were predicted from the empirical formulae of Andrews [11]. Austenite formed during intercritical austenitizing was assumed to transform into martensite. The martensite volume fraction was determined by point counting on the metallographic sections etched in 2% nital.

Based on the results of the preliminary investigation, specimens 10 mm × 10 mm × 5 mm thick machined from the bottom section of Y-block of as cast structure A were intercritically austenitized at various temperatures of 795 and 815 °C for 20 min (these temperatures corresponds to ~24.7 and ~62% austenite volume fraction) (see Fig. 1). The specimens were then rapidly transformed to a salt bath containing 50% KNO_3 + 50% $NaNO_3$ held at the 365 °C for austempering for various times to produce DMS with different ausferrite volume fractions (AFVF) in ferrite matrix. Throughout these heat treatments, the temperature of

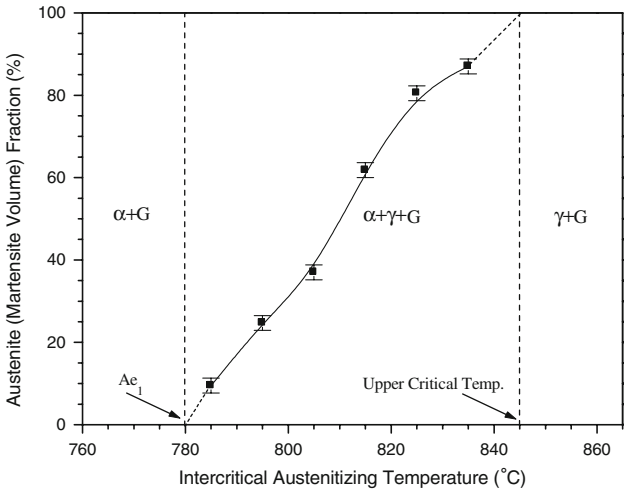

Fig. 1 Dependence of the austenite (martensite at room temperature) content on intercritical austenitizing temperature (phase volume fractions obtained experimentally are not represented exactly because true equilibrium was not reached during the intercritical heat treatment)

Table 1 Chemical composition of unalloyed ductile iron used (wt%)

C	Si	Mn	P	S	Cr	Mo	Ni	Al	Co
3.50	2.63	0.318	0.0190	0.009	0.031	0.0421	0.0423	0.003	<0.001
Cu	Nb	Ti	V	W	Pb	Sn	Mg	Sb	Fe
0.0552	<0.002	<0.0120	<0.001	0.005	<0.0002	0.0058	0.0471	0.0055	Balance

the each specimen was monitored by a thermocouple spot-welded to the centre of one of its faces.

The specimens were coded according to starting microstructure and ICAT. For example, in the specimen code A815, A stands for starting microstructure and 815 for ICAT. The proportions of the constituents present were determined by point counting on etched (Nital and chromate) metallographic sections. Between 1,000 and 2,000 points were counted to keep the standard error of the volume fraction of phases below 6%. The nodule count and ferrite grain size of cast structure were 195 mm^{-2} and 53.14 μm, respectively.

The high-carbon austenite and ferrite volume fractions in all specimens were measured by X-ray diffractometry following the standard procedure [12]. X-ray diffraction profiles were obtained on a Brucer D8 X-ray diffractometer at 40 kV and 20 mA using monochromated Cu Kα radiation. The samples were scanned in the 2θ range of 40–100°at a scanning speed of 0.05°/min. The integrated areas of both austenite (220) and (311) and ferrite (211) peaks were used for determination of volume fraction of austenite and ferrite. The carbon concentration in the austenite was calculated from its lattice parameter using a relationship of Roberts [13]. The bainitic ferrite volume fraction was calculated by substituting the sum of the proeutectoid and new ferrite content calculated by point counting from the X-ray analysis result of the total volume percent of the ferrite. The mean ferrite particle size in conventional ADI were determined from the breadth of {211} peaks of ferrite using the Scherrer formula [14]. The proportions of phases determined by point counting and X-ray analysis are listed in Table 2.

Results and discussion

Microstructures

The nucleation and growth of the austenite during intercritical austenitizing

Starting microstructure of the as cast material had proeutectoid ferrite + graphite structure (Fig. 2). On heating starting ferritic microstructure A (as cast) to the ICAT, the austenite (martensite at room temperature) nucleated preferentially along the previous ferrite/ferrite grain boundaries which are located in the eutectic cell boundary region (Figs. 3a, 4a, 5a) and then grew into surrounding the ferrite (Figs. 3b, 4b, 5b) to achieve an equilibrium volume fraction, as defined by the lever rule. In this stage, austenite growth rate is

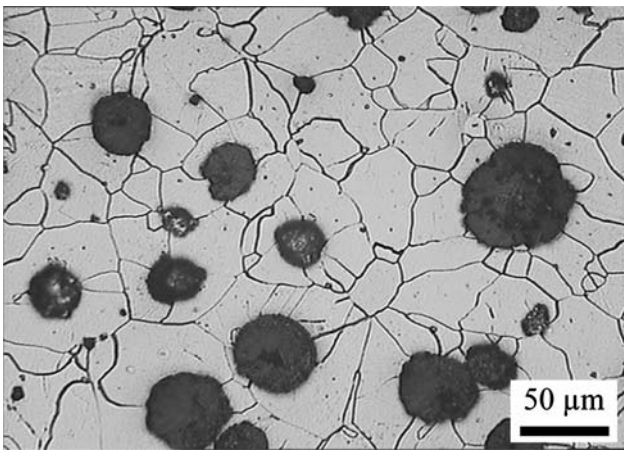

Fig. 2 Microstructure of the as cast material. Etchant: 2% nital

Table 2 Results of metallographical measurements (average values ± 3%)

Specimen code	Austempering time (min)	Proeutectoid ferrite grain size (μm)	Ferrite mean particle size (μm)	Marten. content (vol%)	New ferrite content (vol%)	Proeutectoid ferrite content (vol%)	Bainitic ferrite content (vol%)	High-carbon austenite content[a] (vol%)
A795	30	45.3	–	14.2	1.5	75.3	5.9	3.1
	60	43.5	–	6.6	4.7	75.3	7.6	5.8
	120	42.6	–	0	7.7	75.3	8,9	8.1
	180	41.4	–	0	9.7	75.3	7.9	7.1
A815	30	30.5	–	38.2	7.4	38.2	8.3	7.9
	60	30.8	–	23.2	10.2	38.2	14.6	13.8
	120	28.7	–	0	14.6	38.2	24.7	22.5
	180	27.5	–	0	15.1	38.2	24.4	22.3
C900	30	–	0.8865	52.6	–	–	28.1	19.3
	60	–	0.9545	33.6	–	–	37.9	28.5
	120	–	1.0049	5.5	–	–	55.2	39.3
	180	–	1.0967	0	–	–	62.2	37.8

[a] High-carbon austenite contents were obtained from XRD analyses

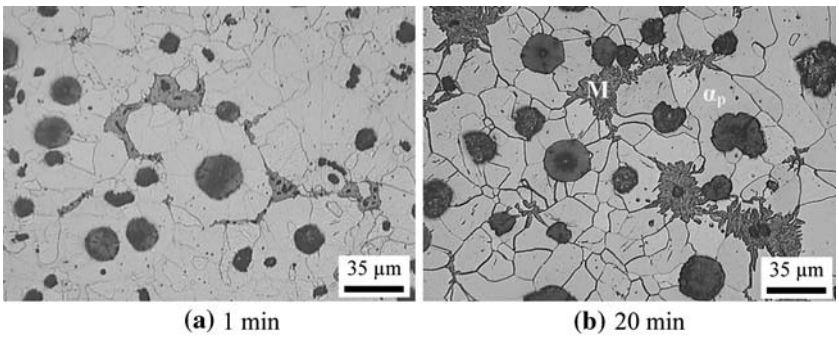

Fig. 3 Micrographs of the specimen A795 partially austenitized at the intercritical temperature of 795 °C for 1 min (**a**) and 20 min (**b**) and then water quenched. Etchant: 2% nital. M: martensite; α_p: proeutectoid ferrite

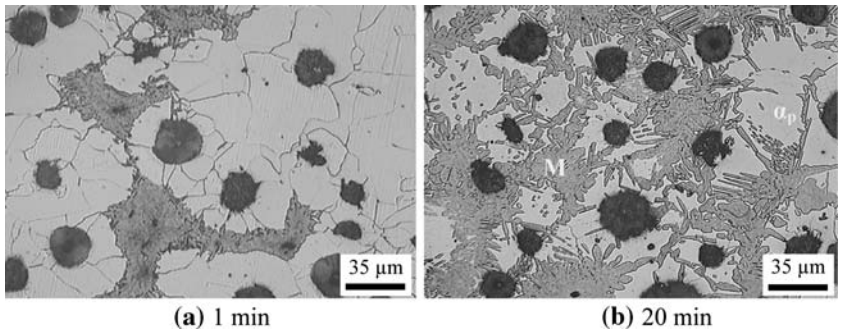

Fig. 4 Micrographs of the specimen A815 partially austenitized at the intercritical temperature of 815 °C for 1 min (**a**) and 20 min (**b**) and then water quenched. Etchant: 2% nital. M: martensite; α_p: proeutectoid ferrite

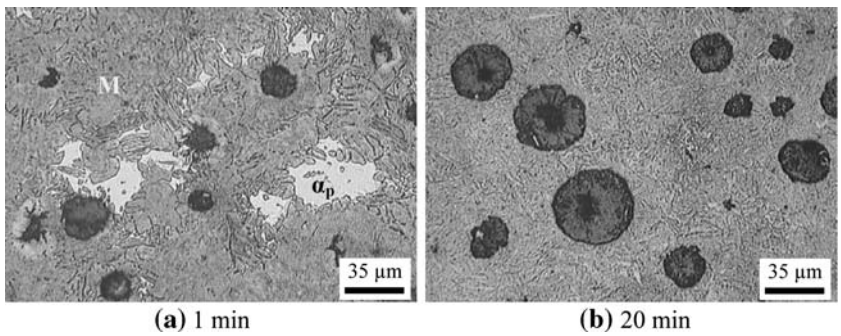

Fig. 5 Micrographs of the specimen C900 fully austenitized at 900 °C for 1 min (**a**) and 20 min (**b**) and then water quenched. Etchant: 2% nital. M: martensite; α_p: proeutectoid ferrite

controlled by carbon due to paraequilibrium conditions (short austenitizing time).

Some alloying elements like Si and Mn are inherently present in ADI. It is already known that Si concentrates near a graphite nodule and Mn partitions into a eutectic cell boundary [5]. Mn reduces the activity of the carbon and encourages austenite nucleation (an austenite stabilizer). Therefore it is reasonable to assume that the eutectic cell region is the most potent site for austenite nucleation. The reason for the absence of formation of austenite near graphite nodules may be attribute to the effect of Si segregation on the reduction of the austenite formation rate.

An increase of the austenitisation time for the series A increases the amount of austenite and encourages austenite formation at ferrite grain boundaries at the same eutectic cell region. An isolated or continuous network of austenite formed along the eutectic cell boundaries depending on the ICAT as shown in Figs. 3 and 4. In this figures the microstructure consist of the proeutectoid ferrite and martensite. As mentioned before, austenite formed during the intercritical austenitizing was assumed to transform into martensite because the water-quenching rate is fast enough for transformation of all austenite present into martensite.

Asymmetrical growth appeared to be characteristic of the austenitization at low temperatures with an initial ferrite microstructure (Fig. 3b). At the high ICAT, preferential growth of the austenite parallel to ferrite grain boundaries become less obvious due to domination of bulk diffusion (Fig. 4b).

The austenite decomposition during austempering

During the austempering process, ADI goes through a two-stage transformation reaction. In the first stage the

austenite γ decomposes into bainitic ferrite α_b and high-carbon austenite γ_{hc} (retained austenite or transformed stable austenite)

$$\gamma \rightarrow \alpha_b + \gamma_{hc} \text{ (stage I)}$$

During the second stage, this supersaturated austenite further decomposes into bainitic ferrite and carbides

$$\gamma_{hc} \rightarrow \alpha_b + \text{carbides (stage II)}$$

As the treatment time increase the amount of austenite isothermally transformed to high-carbon austenite and ferrite increases leading to enrichment of the remaining austenite by carbon rejection. The effect of carbon rejection in stabilizing the remaining austenite becomes much more pronounced at the austenite does not transform when cooled to room temperature. Low-carbon austenite (this transforms into martensite on cooling to room temperature) from stage I reaction and carbide from stage II reaction are detrimental to ductility and toughness [15–26]. Consequently, the desired microstructure of the ADI is ferrite and high-carbon austenite, commonly called ausferrite. This desired ausferrite microstructure is obtained at the austempering time interval between the end of stage I and at the beginning of stage II reactions. This austempering time interval can be referred to as the processing window. Ductile cast iron with this desired ausferrite microstructure displays optimum mechanical properties [10].

An example of the sequence of microstructural changes as a function of time observed during austempering in the present study and show the features described above (Fig. 6). In this specimen after austempering at 365 (C for 1 min; a small amount of ausferrite was evident in the parent austenite area formed during intercritical austenitizing (Figs. 6a, 7a). The bainitic ferrite has started to form preferentially at proeutectoid ferrite/austenite and parent austenite boundaries located in eutectic cell areas. Mainly martensitic structure formed from the low-carbon untransformed austenite, when it was air cooled to room temperature from the austempering temperature and the formation of martensite as followed by the formation of bainitic ferrite. In these series typical ausferritic structure (bainitic ferrite and high-carbon austenite) became more obvious with increasing austempering time as shown in Figs. 6a–d and 7d. The desired DMS composed of the proeutectoid ferrite + ausferrite was obtained after austempering for approximately 120 min (Fig. 6d).

In these DMSs, the sum of the parent austenite transformation products of ausferrite (bainitic ferrite + high-carbon austenite) should be equal to the volume fraction of parent austenite present at the ICAT. However in the present study it was found out that some percentage of the parent austenite transformation products was missing. For example at ICAT of 815 °C, the austenite and proeutectoid ferrite volume

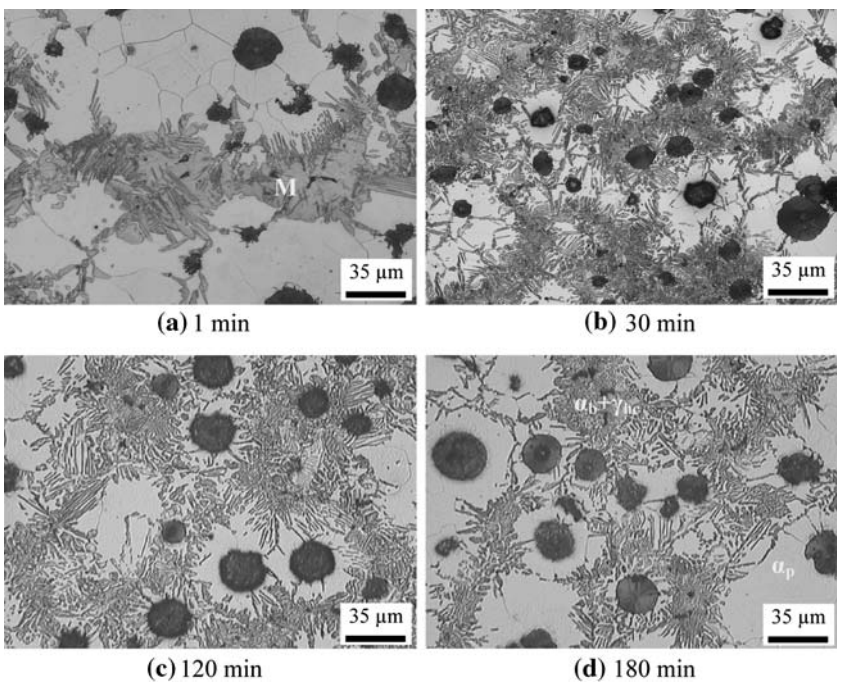

Fig. 6 Microstructural changes in the specimen A815 during various austempering time of (**a**) 1 min, (**b**) 30 min, (**c**) 120 min and (**d**) 180 min at 365 °C after intercritical annealing at 815 °C. Etchant: 2% nital. $\alpha_b + \gamma_{hc}$: ausferrite (bainitic ferrite + high-carbon austenite); α_p: proeutectoid ferrite

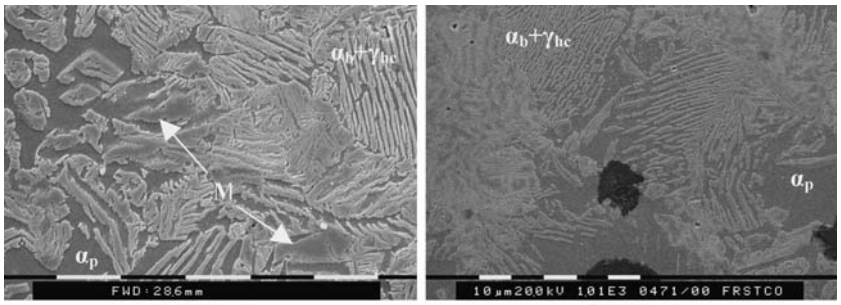

(a) 15 min **(b)** 30 min

Fig. 7 SEM micrographs of microstructural changes in the specimen A815 during various austempering time of (**a**) 1 min and (**b**) 30 min at 365 °C after intercritical annealing at 815 °C. Etchant: 2% nital. $\alpha_b + \gamma_{hc}$: ausferrite (bainitic ferrite + high-carbon austenite); M: martensite, α_p: proeutectoid ferrite

fractions were equal to ~61.8 and ~38.2%, respectively (see Fig. 2). After austempering for 120 min from 815 °C, nital etching revealed that the microstructure consisted of proeutectoid ferrite, bainitic ferrite and high-carbon austenite (Fig. 6d). On this nital etched sample metallographic measurement showed that sum of the parent austenite products of bainitic ferrite and high-carbon austenite was equal to ~47.2%. This means that ~14.6% of austenite transformation product was missing.

The X-ray analyses of this sample showed that the microstructure consisted of ~22.5% of high-carbon austenite and ~77.5% of ferrite. As a result of this analysis it was found out that the missing austenite transformation product was ferrite, but the type of this missing ferrite was not clear. To reveal the type of this missing ferrite, the chromate etching technique invented by Lawson et al. [26] was used. This etching technique was used by several investigators [25–34] to reveal new ferrite in dual-phase steels which were intercritically annealed at ICAT and then cooled to room temperature at the variety of cooling rates. In the present study the chromate etching showed that the epitaxial ferrite as the bright, white constituent same as in dual-phase steels as shown in Fig. 8d.

The austenite transformation during austempering following intercritical austenitizing is different from that after normal austenitizing in two respects. First, in the dual matrix heat treatment austenite volume fraction and its carbon content are determined by the ICAT. Under paraequilibrium condition (short intercritical austenitizing time) carbon, but not substitutional alloying elements segregates and determines phase proportions and compositions. Secondly a nucleation step is not required for new ferrite to form, because the proeutectoid ferrite (the old ferrite) present during ICAT can grow epitaxially into the austenite [26–35].

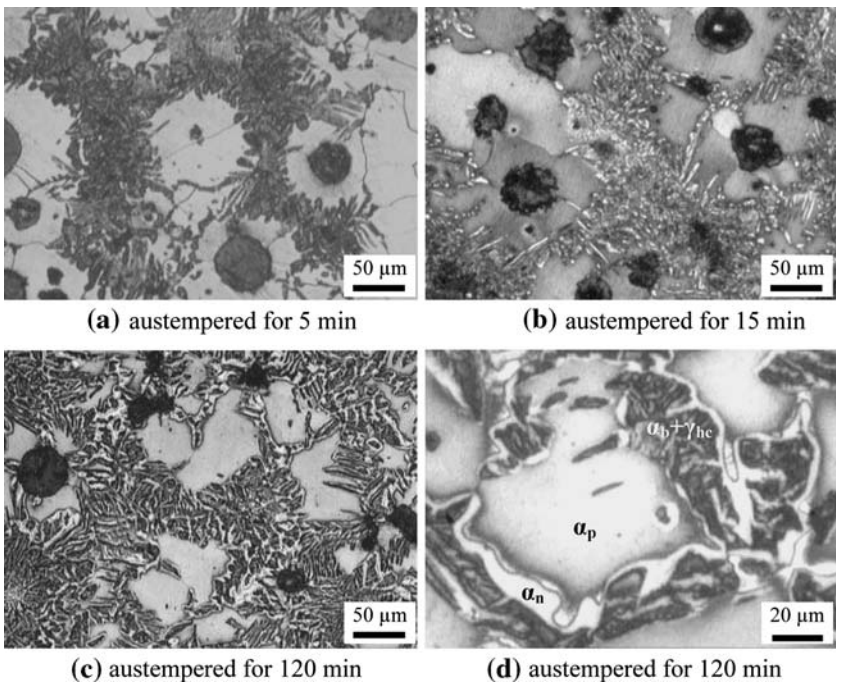

(a) austempered for 5 min **(b)** austempered for 15 min

(c) austempered for 120 min **(d)** austempered for 120 min

Fig. 8 Microstructural changes in the specimen A815 during various austempering time of (**a**) 5 min, (**b**) 15 min, (**c**) 120 min and (**d**) 120 min at 365 °C after intercritical annealing at 815 °C. Etchant: 2% nital. New ferrite revealed as bright white areas after etching in hot chromate reagent. $\alpha_b + \gamma_{hc}$: ausferrite (bainitic ferrite + high-carbon austenite); α_p: proeutectoid ferrite; α_n: new ferrite (epitaxial ferrite)

Following the bainitic ferrite formation, epitaxial ferrite growth occurred during austempering at prior austenite–ferrite boundaries without a need for a nucleation step. The interface between the new and proeutectoid ferrite delineated the size of the austenite volumes formed during intercritical austenitizing. The decomposition of austenite always proceeded by epitaxial growth on the proeutectoid ferrite into austenite without a nucleation step as shown in Fig. 8d.

These figures also show that during austempering, bainitic ferrite formed first and new ferrite formation followed this after approximately 15 min austempering and its amount increased with increasing austempering time until remaining austenite became richer enough in carbon for stabilization as shown in Fig. 8.

In all specimens, after approximately 120 min austempering, martensite almost disappeared and between 120 and 180 min austempering, volume fraction of bainitic ferrite, new ferrite and high-carbon austenite remained almost unchanged. This austempering time from 120 to 180 min may be interpreted as the useful range or process window for present ADI to obtain ideal bainitic ferrite and high-carbon austenite structure. This is well supported by the X-ray diffraction studies where the relative amounts of ferrite and austenite were determined (Table 2). Since austempering time between 120 and 180 min is well within the process window.

Quantitative microstructure maps

Examples of the result of quantitative metallographic analysis of the series A specimens are shown in Fig. 9 in the form of microstructure maps. The volume fractions of transformed austenite, martensite, new ferrite and bainitic ferrite are not independent variables, their sum being equal to the volume fraction of parent austenite present at the ICAT. Increasing the austempering time causes new ferrite, bainitic ferrite and high-carbon austenite to displace martensite.

The presence of new ferrite in the ADI from the ICAT range has not yet been reported. The formation of the new ferrite in the ductile cast iron may be an important feature of the transformation characteristics of this material. Due to the nature of new ferrite formation, it is believed that the new ferrite contains fewer impurities than the proeutectoid ferrite [13, 36]. The microstructural difference between new ferrite and proeutectoid ferrite was observed by Geib et al. [28] in a transmission electron microscopy study of intercritically annealed, Nb microalloyed HT12 steel. They reported that a precipitate structure developed in the proeutectoid ferrite during intercritical austenitizing.

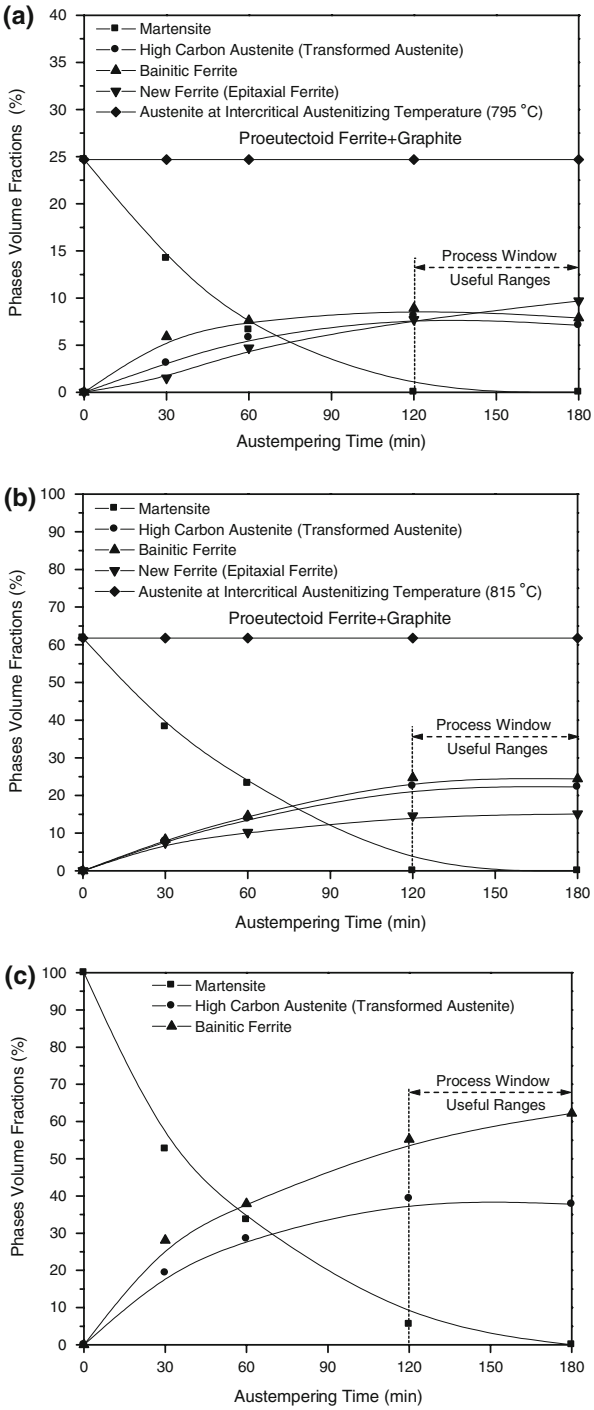

Fig. 9 Quantitative microstructure maps of the A795 (**a**), A815 (**b**) and C900 (**c**) specimens showing the effect of austempering times on the microstructure (the proeutectoid ferrite (old ferrite) corresponds to the presence of original ferrite at intercritical austenitizing temperatures in (**a**) and (**b**)

On subsequent cooling the periphery of the austenite pool transformed to ferrite by an epitaxial growth mechanism. No precipitation occurred in this new

ferrite. It has also been reported that after slow cooling, the new ferrite had a lower transformation-induced dislocation density than the proeutectoid ferrite. With respect to the proeutectoid ferrite; the precipitation free new ferrite is expected to have grater ductility and lower strength. One of the present authors also showed that ductility increased with increasing new ferrite content in dual-phase steels [30–33].

Figure 9a and b also shows that the new ferrite content increased with increasing austempering time in austempered specimens from ICAT range. However the new ferrite in the specimen C900 austempered from single-phase (γ) region was not observed (Fig. 9c). The reason for the absence of the new ferrite in the specimens C900 is explained in Sect. 3.3. As mentioned previously, increasing the ICAT increases the parent austenite volume fraction and its carbon content. Therefore the parent austenite formed at higher ICAT has a higher carbon content than parent austenite formed at low ICAT. In turn this parent austenite carbon content is expected to have an influence on austenite stabilization or transformation kinetics during the austempering.

The microhardness variation in martensite with ICAT in the quenched samples from ICAT range is given in Fig. 10. Variation in the microhardness of martensite is a good indication of austenite carbon content due to diffusionless nature of martensite transformation from the austenite. The result of the XRD analyses for measuring the variation of austenite carbon content with austenitizing temperature at the constant 120 min austempered time is given in Fig. 11.

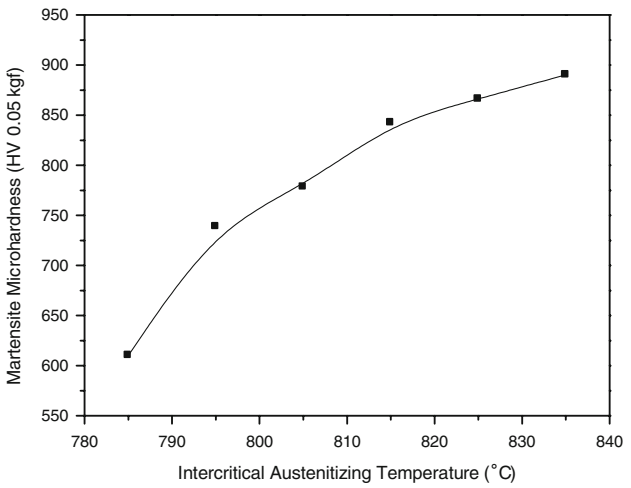

Fig. 10 The relationship between the ICAT and martensite microhardness of intercritically annealed and then water quenched specimens

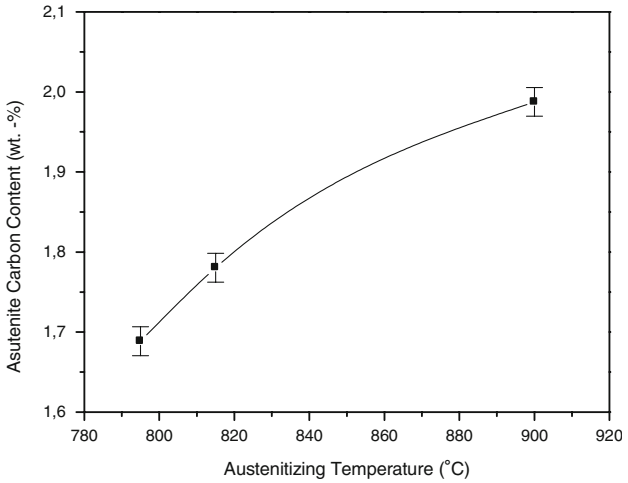

Fig. 11 At the constant 120 min austempering time, XRD analyses of specimens showing the variation of austenite carbon content with austenitizing temperature

The austenite carbon content increased with increasing austenitizing temperature. This result is in good agreement with existing literature [13, 36].

As is well known, the austenite stabilization in the ADI has a vital importance to determine the mechanical properties. In several investigations [37–41], this feature was explained by the means of process windows which do not show the effect of quantitative phase variations with austempering times on the austenite stabilization as in a microstructure map (Fig. 9).

Effect of the austenite volume fraction and its carbon content on the austenite stabilization and the new ferrite formation during austempering

The microstructure maps shown in Fig. 9 were interpreted in the form of austenite → new ferrite and austenite → high-carbon austenite diagrams, as in Fig. 12. In the present experiments, for the same austempering times, austempered samples from the highest ICAT produced a grater high-carbon austenite volume fraction than those samples austempered from low ICAT (Figs. 12 and 13). These results may be caused from the higher austenite and its carbon content formed during the intercritical austenitizing as predicted by the lever rule. This suggests that for a given austempering time the average new ferrite growth rate will be considerably slower for the austenite with higher carbon content than austenite with low-carbon content ones. Therefore, less new ferrite and much higher carbon austenite will form and this difference will increase with increasing the ICAT. That is why new ferrite may be absent in the specimen

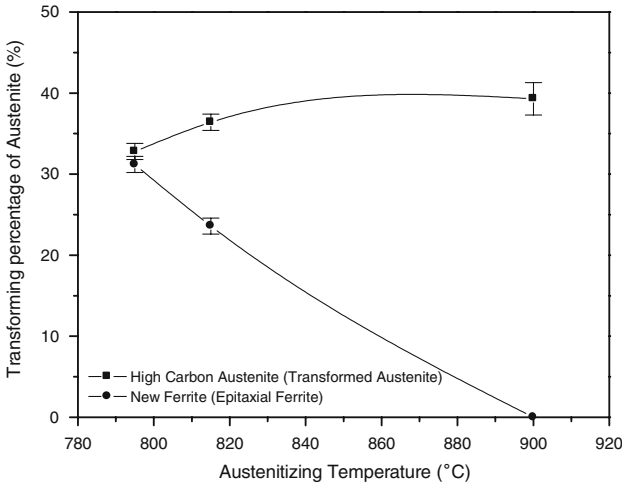

Fig. 12 Transforming percentage of austenite to high-carbon austenite and new ferrite for austenite content of specimen of A795, A815 and C900

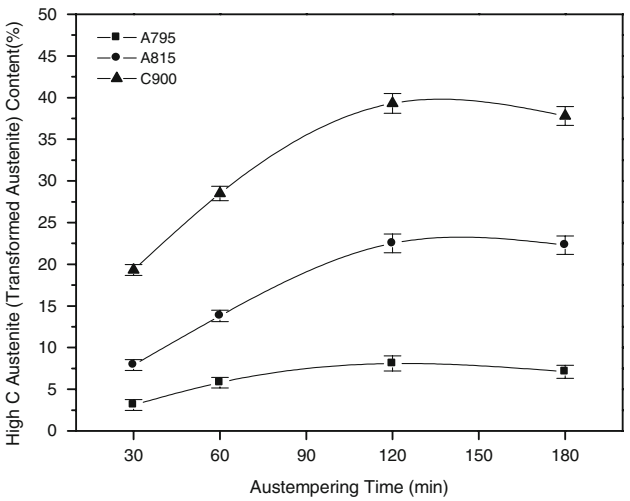

Fig. 13 The variation of high-carbon austenite (transformed austenite) content with austempering time

C900 with higher carbon content austempered from single-phase (γ) region.

The new ferrite growth rate seems to be a complex function of the austempering time, carbon diffusion rate and carbon concentration in the austenite at the α/γ interface. The carbon content has a large effect in reducing new ferrite growth rate. It is noted that the new ferrite growth must be very sensitive to carbon concentration in the austenite; much more new ferrite formed in austenite obtained at 795 °C than in that obtained at 815 °C (Fig. 12). This result may arise from the sensitivity of new ferrite growth rate to increasing carbon concentration in austenite as the austenite shrinks during austempering. As mentioned before the austenite carbon content increases with increasing ICAT (Fig. 11) and austempering time which means that the variation in the carbon content of austenite during the austempering of sample austempered from ICAT range is influenced not only by austempering time but also by the ICAT.

Conclusions

1. The total volume fraction of the transformed phases is approximately constant for all austempering times after rapidly transforming samples from a particular intercritical temperature.
2. New ferrite is an identifiable, controllable parameter in ductile cast irons austempered from the ICAT.
3. The carbon content of the austenite has a large effect in reducing the new ferrite growth rate.
4. New ferrite content depends on the ICAT and austempering time. The new ferrite content increases with increasing ICAT and austempering time.
5. Martensite content gradually decreases and finally disappears with increasing the austempering time while the transformed austenite content decreases and new and acicular ferrite contents increases.
6. Transformation percent of the austenite to new ferrite increases with decreasing the ICAT.

Acknowledgements The authors wish to acknowledge the financial supports of Gazi University Scientific Research Fund (Project no 07/2003–41) and DPT (The State Planning Organization of Turkey, Project no. 2001 K120590). The author is also indebted to ALFA Casting Company for Castings (Ankara, Turkey) and to Ankara Nuclear Research and Education Center (TAEK-ANAEM) for providing X-ray facilities.

References

1. Voigt RC, Eldoky LM, Chiou HS (1986) AFS Trans 94:645
2. Rashidi AM, Moshrefi-Torbati M (2000) Mater Let 45:203
3. Cerah M, Kocatepe K, Erdogan M (2005) J Mater Sci 40:1
4. Aranzabal J, Serramoglia G, Rousiere D (2003) Int J Cast Met Res 16:185
5. Kobayashi T, Yamamoto H (1988) Metall Mater Trans A 19A:319
6. Kobayashi T, Yamada S (1996) Metall Mater Trans A 27A:1961
7. He ZR, Lin GX, Ji S (1997) Mater Charact 38:251
8. Hafiz M (2001) Z Metallkd 11:1258
9. Kazerooni R, Nazarboland A, Elliot R (1997) Mater Sci Technol 13:1007
10. ASM metals handbook (1991) Heat treating, vol 4. Metals Park, Ohio, p 683

11. Andrews KW (1965) J Iron Steel Inst 203:721
12. Cullity BD (1978) Elements of X-ray diffraction. Addison-Wesley, USA, p 412
13. Roberts CS (1953) Trans AIME 197:203
14. Cullity BD (1974) Elements of X-ray diffraction. Addison Wesley: Reading, MA, p 102
15. Labreque C, Gagne M (1998) Can Metall Q 38:343
16. Trudel A, Gagne M (1997) Can Metall Q 36:289
17. Darwish N, Elliot R (1993) Mater Sci Technol 9:572
18. Yazdani S, Elliot R (1999) Mater Sci Technol 15:531
19. Zhao W, Wang G (1999) J Mater Proc Technol 95:27
20. Bahmani M, Elliot R, Varahram N (1997) J Mater Sci 32:4783
21. Mallia J, Grech M, Smallman RE (1998) Mater Sci Technol 14:452
22. Putatunda SK (2001) Mater Manuf Processes 16:245
23. Bayati H, Elliot R, Lorimer GW (1995) Mater Sci Technol 11:776
24. Aranzabal J, Gutierrez I, Urcola JJ (1994) Mater Sci Technol 10:728
25. Baydoğan M, Çimenoğlu H (2001) Scand J Metall 30:391
26. Lawson RD, Matlock DK, Krauss G (1980) Metallography 13:71
27. Huppi GS, Matlock DK, Krauss G (1980) Scripta Mater 14:1239
28. Geib MD, Matlock DK, Krauss G (1980) Metall Trans A 11A:1683
29. Lawson RD, Matlock DK, Krauss G (1981) In Kott RA, Bramfitt BL (eds) Fundamentals of dual-phase steels. AIME, New York, p 347
30. Erdogan M (2002) J Mater Sci 37:3623
31. Erdogan M, Priestner R (1999) Mater Sci Technol 15:1273
32. Erdogan M, Priestner R (2002) Mater Sci Technol 18:369
33. Erdogan M (2003) Scripta Metall 48:501
34. Sarwar M, Priestner R (1996) J Mater Sci 8:2091
35. Matlock DK, Krauss G, Ramos LF, Huppi GS (1979) In: Kott RA, Morris JW (eds) Structure and properties of dual phase steels. AIME, New York, p 62
36. Rundman KB, Klug RC (1982) AFS Trans 90:499
37. Moore DJ, Rouns TN, Rundman KB (1985) AFS Trans 103:705
38. Hayrynen KL, Moore DJ, Rundman KB (1990) AFS Trans 127:471
39. Darwish N, Elliot R (1993) Mater Sci Technol 9:882
40. Bayati H, Elliot R (1995) Mater Sci Technol 11:284
41. Hamid Ali AS, Elliot R (1997) Mater Sci Technol 13:24